AHEAD Workpackage 8
JRA X-ray optics

Deliverable D8.6 – D36

BEaTriX (Beam Expander X-ray Testing facility) final design report

Written by	Daniele Spiga (INAF/OAB)	
Checked by	Vadim Burwitz (MPE)	
Distribution List	AHEAD Management Team Vadim Burwitz WP8.0, WP8.1, WP8.3 Dick Willingale WP8.1 Rene Hudec WP8.1 Daniele Spiga WP8.1, WP8.2	
Distribution Date	Draft version	Sept 28, 2016
	Final version	Oct 12, 2016

1. MOTIVATIONS

Parallel and wide X-ray beams are required for several applications: wide-aperture X-ray optics, diffractive lenses, medical imaging, and X-ray tomography to name a few. As of today, broad and quasi-parallel beams can be obtained using distant, powerful, and diverging sources. However, large X-ray facilities operating in high vacuum are required - such as MPE/PANTER,[1] or the longest beamlines at the largest synchrotron light sources such as BL20B2 at SPring-8[2] - to efficiently test large aperture X-ray optical systems, or at least a significant sub-aperture of them. This can pose a challenge for X-ray tests of optical X-ray assemblies based on a modular approach such as the ATHENA X-ray telescope.[3] ATHENA's optical system will have an outer diameter of 3 m, a 12 m focal length, a 2 m^2 effective area at 1 keV, an angular resolution better than 5 arcsec HEW (*half-energy-width*) at 1 keV, and better than 10 arcsec at 6 keV. In order to reach these performances, more than 1000 X-ray Optical Units (XOUs) based on Silicon Pore Optics[4] have to be manufactured, tested, qualified before the accurate alignment and integration into the supporting structure. Each pore in each XOU reproduces the Wolter-I (parabola+hyperbola) configuration and, owing to the wedged ribs, all the pores in an XOU converge to focus. Each XOU integrated in ATHENA has to be accurately co-axially and co-focally aligned, but some alignment error is unavoidable. Hence, each individual, flight-grade XOU has to be characterized by an angular resolution much better than 5 arcsec, and only the most performing XOUs out of the industrial production line can be selected to be integrated. Indeed, because of the small pore size (a few mm^2), metrological tests on the XOU stacks are extremely difficult, and a reliable qualification test can be a direct measurement of the optical performances in X-rays. This also offers the possibility to reliably align the parabolic and the hyperbolic stack of the XOU, as the maximization of the effective area - corresponding to the best align condition - can be checked at-wavelength. Tests is UV light would also enable this alignment, but they would be heavily affected by aperture diffraction caused by the rib/membrane obstruction[5] which would also hide the PSF shape that would be expected in X-rays.

To date, X-ray tests of SPO XOUs are performed in pencil beam setup at the PTB lab of the BESSY synchrotron light source,[6] but the point spread function (PSF) measurement requires reconstruction because only a pore at a time can be illuminated, and the complete scan of a XOU aperture is time consuming. A measurement at PANTER would in contrast enable a true full-illumination test, possibly compensating the beam divergence by the application of a diffractive X-ray lens.[7] However, PANTER is a very large facility and cannot be routinely employed to perform the functional test of 1000 XOUs. Finally, both for BESSY and PANTER, the testing facility cannot be moved near the XOU production site, which imply a continuous module transportation across Europe.

We have therefore designed[8] a compact facility to generate a broad, parallel, uniform, monochromatic, and polarized X-ray beam, named BEaTriX[9] (*Beam Expander Testing X-ray facility*) to the specific end of testing ATHENA XOUs in full illumination, with reduced costs and in a time short enough to sustain a production rate of a few XOU modules per day, and so return a prompt feedback to the manufacturer. BEaTriX is being constructed at INAF/OAB, to be possibly replicated at the industrial production site of the XOUs. Specifications include:

i) an X-ray beam wider than 90 mm and higher than 55 mm to fully illuminate the largest apertures of XOUs;
ii) very low residual divergence (< 1.5 arcsec HEW), aiming to reliably characterize XOU PSFs (*point spread functions*) with an intrinsic HEW of 3-4 arcsec. The collimation in the vertical plane is especially important because it corresponds to a beam spread in the XOU incidence plane, in which the PSF is elongated by longitudinal profile errors and by the surface roughness;
iii) high beam uniformity (better than 10%) to equally characterize the entire optical surface;
iv) highly monochromatic energy, selectable between 1.5 keV and 4.5 keV;
v) compact size to fit a small laboratory (6 m x 15 m), and reduce the test chamber evacuation time.

In this report we review an updated project design[10] of BEaTriX (Sect. 2) and show the advancement status of the project (Sect. 3).

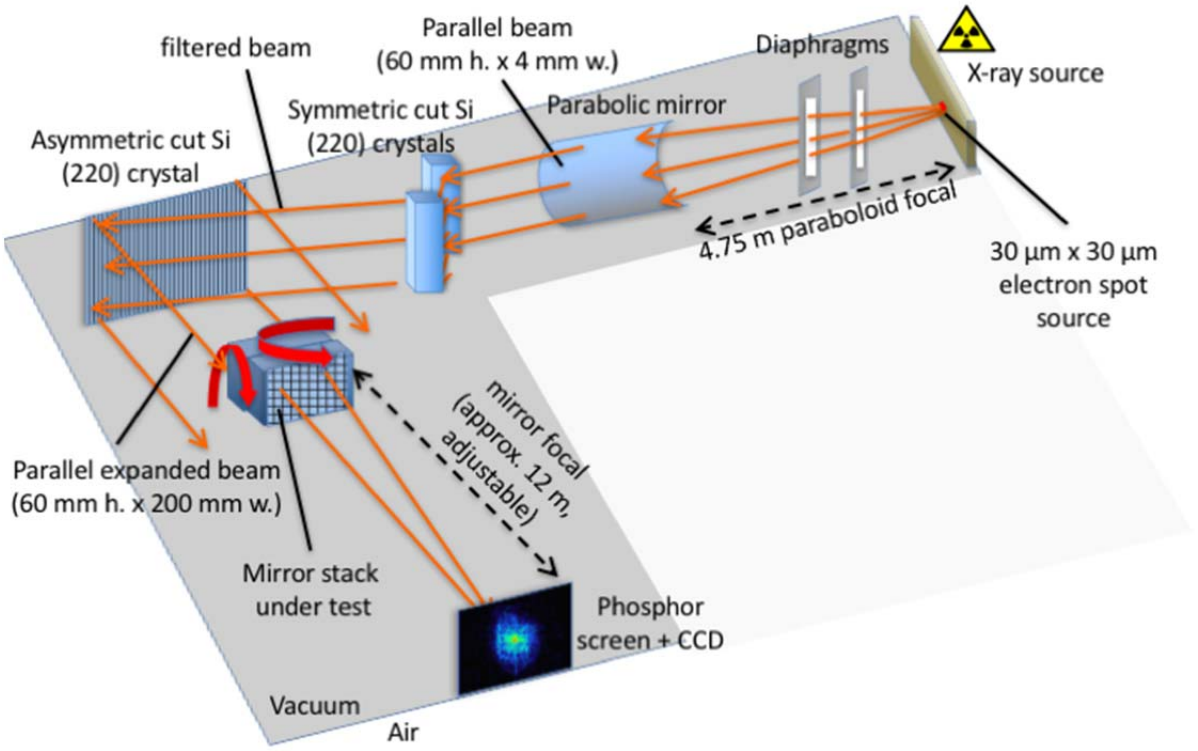

Fig. 1: schematic design of the BEaTriX facility in the 4.5 keV setup. The beam diverging from a microfocus X-ray source is collimated by a precisely figured paraboloidal mirror (Fig. 2) with the source in its focus. The beam has now a 4 mm (h.) x 60 mm (v.) size and the subsequent diffraction operated by a pair of symmetric silicon crystals precisely isolates the 4.51 keV fluorescence line (Fig. 3). The horizontal expansion of the beam is operated by an asymmetrically-cut silicon crystal with respect to the (220) planes (Fig. 4). The expanded beam (200 mm x 60 mm) can be used to illuminate the aperture of the focusing device under test, and the focus is directly observed by means of an imaging detector.

2. PROJECT REVIEW AND DESIGN

2.1. Optical component description

Once completed, BEaTriX will exploit a combination of grazing-incidence mirrors and symmetric/asymmetric diffraction crystals to expand an X-ray beam to the required size. The detailed facility layout, shown in Fig. 1, includes:

1) *A microfocus X-ray source* with either aluminum (1.49 keV setup) or titanium (4.51 keV setup) anode to generate an intense X-ray beam including the fluorescence lines and a bremsstrahlung continuum: the electron spot source has to be extremely small (30 µm x 30 µm) to ensure the required vertical collimation. Microfocus sources of this kind the available on the market: some models generate a copious X-ray flux (on the order of 10^{12} ph/sec/sterad) with a very low power consumption (15 W).
2) *A paraboloidal, grazing incidence mirror* with a 4.75 m focal length (measured from the side nearest to the source) and a 6 cm-high illuminated surface (Fig. 2, left). The X-ray source is located just in the focus of the paraboloid within a ± 1 mm tolerance along the axis and a 50 µm tolerance in the lateral displacement. The mirror is to be coated with a platinum layer (30 nm) and an amorphous carbon overcoating (3 nm) to enhance the low-energy reflectivity[11]. Forming a grazing incidence angle of 0.9 deg, the mirror exhibits high reflectivity up to 6.5 keV (Fig. 2, right). After the reflection, the beam is collimated, parallel, with a vertical size of 6 cm, and a horizontal suitable size of 4 mm[10]. Details on the ongoing fabrication of the paraboloidal mirror are reported in Sect. 3.1.

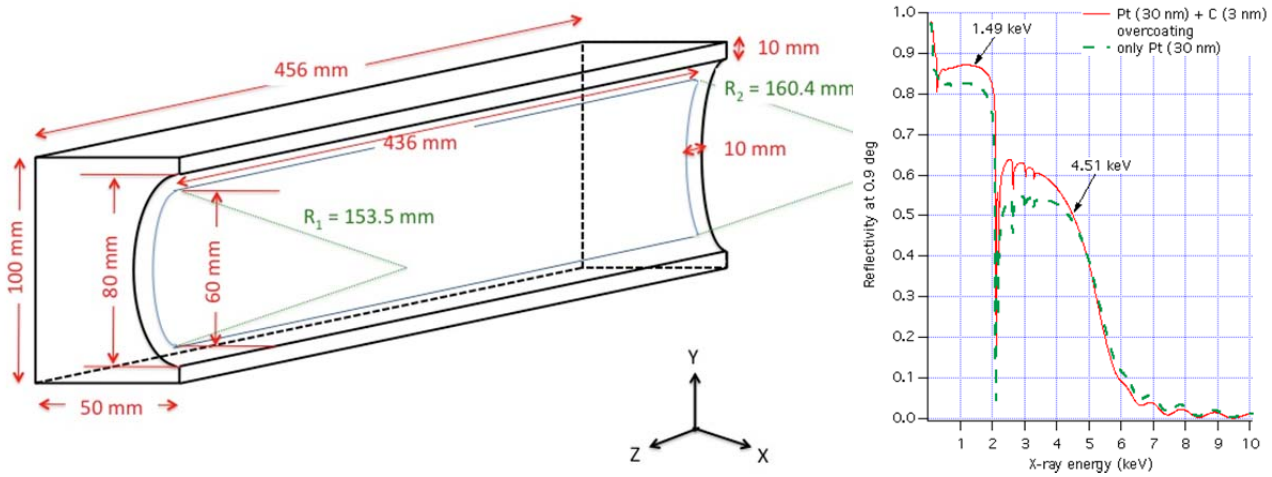

Fig. 2: (left) a drawing of the paraboloidal mirror. The focus is located 4750 mm away from the mirror entrance with curvature radius R_1, in the direction of the positive *z* axis. (right) calculated mirror reflectivity at a 0.9 deg incidence angle.

3) *A pair of symmetrically-cut crystals* (i.e., with diffraction planes parallel to the surface) to filter the Kα line in the X-ray source, but with *no change* in the beam size. For a high collimation of the X-ray beam, excellent (to 0.5 eV FWHM) monochromation is essential. At 4.51 keV, monocrystalline silicon (220) can be used (1.91 Å d-spacing, corresponding to a 45.85 deg Bragg angle) because the rocking curve exhibits a pronounced peak (Fig. 3, red line) reaching a 95% reflectivity in a sharp peak. Higher harmonics - such as (440) – were previously rejected by the collimating mirror. The monochromation can be improved further employing two diffractions in sequence with crystals in parallel interfaces: in this way, the peak region has still high reflectivity, but the reflection tails are suppressed: the combined reflectivity (Fig. 3, black line) has a FWHM of 25 arcsec, but the reflectivity exceeds 80% in a 3 arcsec-wide angular range. This means that, in order to have high diffraction efficiency, the paraboloidal mirror *needs to spread the rays in the incidence plane by less than* $\Delta\theta_B$ *= 3 arcsec*: the filtering efficiency degradation corresponding to this diffraction angle range is < 0.1 eV, close to the natural X-ray line width and not significantly affecting the final beam collimation. Finally, the reflectivity only varies by 9% within this angular range, fulfilling the uniformity < 10% requirement. These considerations imply a 3 arcsec HEW optical quality for the collimating mirror, which shall therefore be figured and polished in compliance to this requirement.
Another advantage offered by this configuration is that the final beam direction is parallel to the initial one and no folded vacuum tube is required to follow the beam at this stage. Finally, we note that the incidence angle is very near the polarization angle, so the beam is not only filtered spectrally, but also strongly *polarized* (97% already after the first diffraction) in the s-plane, i.e., the vertical plane of the facility. While this is not expected to affect the PSF characterization of grazing-incidence mirrors, it can be suited for possible X-ray polarimetry experiments[12].
For the 1.49 keV setup, silicon (220) should be better replaced by ADP (101) - Ammonium Dihydrogen Phosphate, $NH_4H_2PO_4$ (5.32 Å d-spacing, corresponding to a 51.46 deg Bragg angle).

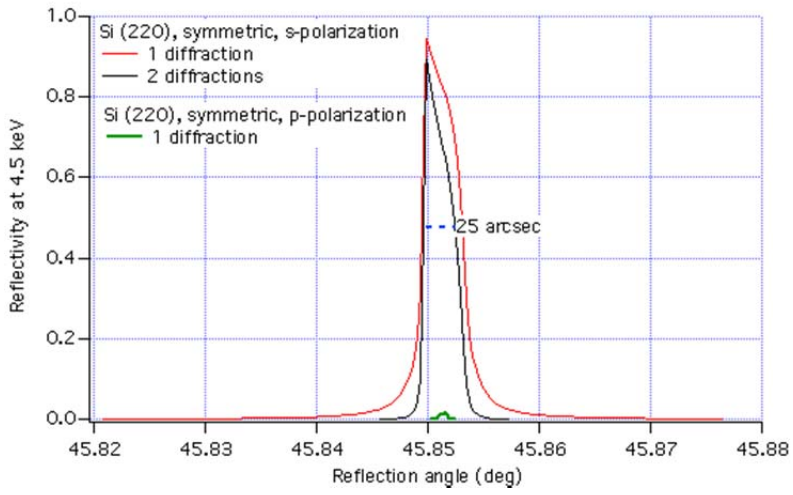

Fig. 3: the (220) rocking curve of the symmetric silicon crystal at 4.5 keV, in single and double diffraction. The incidence angle is very close to the polarization angle and the beam becomes linearly polarized in the tangential plane. Two consecutive diffractions suppress the rocking curve wings and so considerably improve the monochromation.

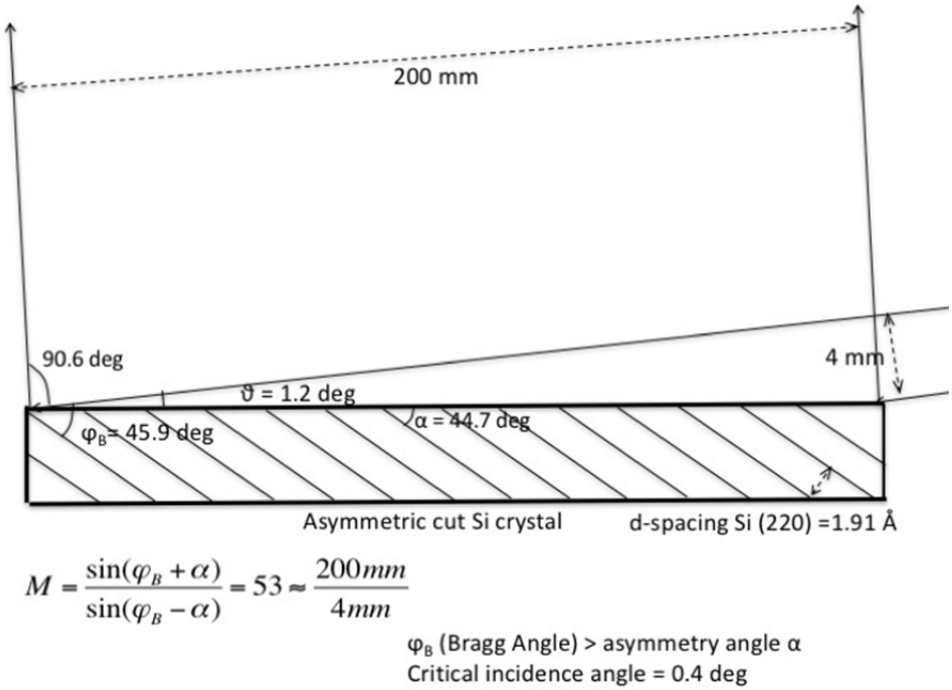

Fig. 4: principle of X-ray beam expansion via an asymmetrically-cut crystal. The incidence angle is larger than the critical incidence angle at 4.51 keV (0.4 deg) on silicon to avoid total external reflection.

4) *An asymmetrically-cut crystal* (i.e., with diffraction planes tilted with respect to the surface[13]) to expand the monochromatic and collimated beam in the horizontal direction. In the 4.5 keV setup, shown in Fig. 4, the silicon crystal has the (220) diffraction planes tilted by 44.7 deg with respect to the outer surface. The beam, with an effective width of 4 mm, impinges in grazing incidence on the crystal surface, but the incidence angle is anyway larger than the critical incidence angle of silicon at 4.51 keV; hence, the total external reflection is suppressed. The 60 mm x 4 mm beam is spread over the crystal surface and is reflected with respect to the tilted (220) planes. Because of the incidence angle close to 45 deg on the Bragg planes, the beam is reflected near a right angle off- surface, and the horizontal beam size is expanded by a factor of 50. The final beam has thereby a size of 60 mm (v.) x 200 mm (h.), fulfilling the initial request, and can be used to fully illuminate the aperture of the XOU under test, with a vertical divergence of 1.3 arcsec (determined by the source size and the mirror focal length) and a horizontal collimation of 1.5 arcsec HEW, determined by the width of the exit rocking curve of the asymmetric crystal. This is shown in Fig. 5, where the reflectivity curve is plotted as a function of the entrance (left) and of the exit (right) angle. Unlike in symmetric geometry (Fig. 3), the exit rocking curve width is 50 times smaller by than the one in entrance; therefore, even if the beam is imperfectly collimated at the exit of the monochromator, the final collimation degree is the one described by the rocking curve width on right side of Fig. 5.

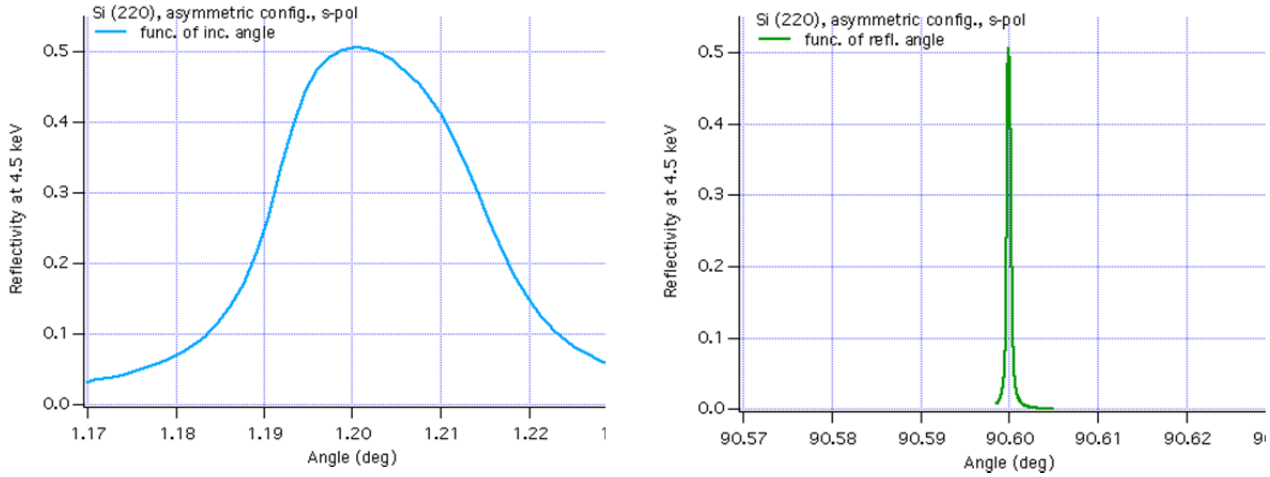

Fig. 5: diffracted intensity by the silicon crystal (220) at 4.5 keV in asymmetric configuration (Fig. 4), as a function of the incidence angle (left) and as a function of the reflection angle (right). The asymmetric diffraction improves the horizontal collimation of the beam to a 2 arcsec FWHM (approx. 1.5 arcsec HEW). The diffracted intensity for the p-polarization is 500 times smaller and is not shown.

5) *A sample alignment stage* to support and precisely align in the X-ray beam the XOU under test. The alignment stage needs two translation motors to move the XOU in the transverse beam section to 1 µm accuracy and three rotation stages to maximize the doubly-reflected beam intensity to 1 arcsec accuracy, a condition corresponding to the best XOU alignment. A more complex system will be obviously required to perform the alignment of the parabolic to the hyperbolic segment of the XOU.
6) *An imaging detector* in the focus of the XOU to directly measure its PSF. To avoid the complication of keeping a camera under vacuum and ease its movement in all directions, the simplest solution is represented by a phosphor window and a CCD sensitive to phosphorescent light to record the image. The camera should have a 10 µm spatial resolution (corresponding to 0.2 arcsec) in order to oversample a PSF a few arcsec wide. The field of the camera should cover approximately 10 arcmin (a 34 mm-sided field at a 12 m distance).

2.2. Outer facility view

Viewed from outside (Fig. 6), BEaTriX is composed of two arms, made of vacuum tubes and chambers, roughly forming an "L" shape and enclosing the optical components listed in Sect. 2.3. The corner corresponds to the asymmetric crystal where the beam is approximately deviated by 90 deg in the horizontal plane. The short arm, approx. 6 m long parallel to the laboratory basement, is responsible for the beam expansion and includes the source and the optical components. The long arm (~13 m) includes the XOU handling stage, followed by a 12 m-long tube that propagates the X-ray focused by the XOU to the focal plane. In order to follow the focused beam - that will be deviated downwards by the double reflection on the XOU – the 12 m long tube shall be tilted in the vertical plane in a 0 – 7.2 deg range (corresponding respectively to the direct beam detection and the angular deviation by the largest radii of ATHENA). The short arm, in contrast, will be steered horizontally to adjust the angle between the two arms when the testing energy is changed, and so satisfy the Bragg law with the crystals in use. Some vacuum joints are flexible to enable the angle setting. All the pipeline will be mounted in a self-bearing structure, with the vacuum tubes counterbalanced with calibrated weight in order to minimize the motor load. The tubes are built modular to enable shorter tubes and intra-focal measurements.

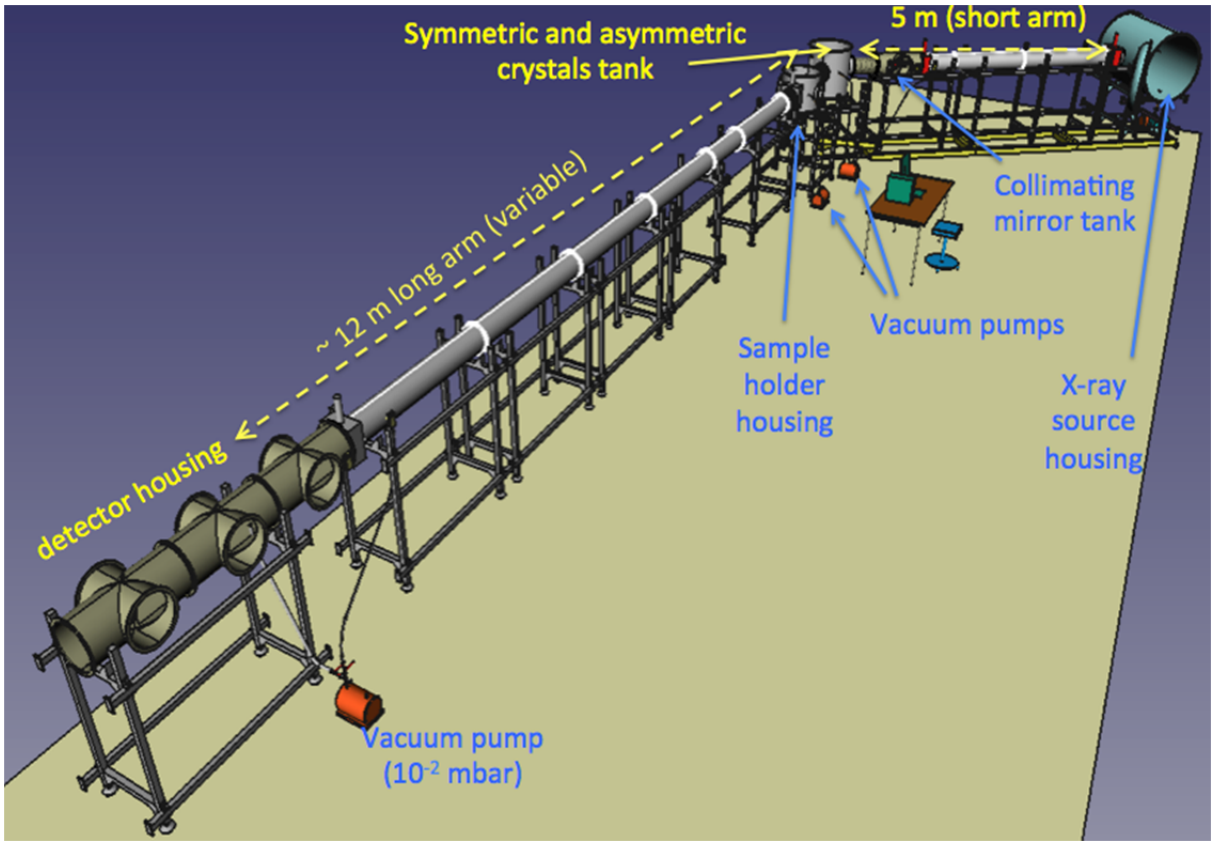

Fig. 6: outer view, simplified design of the BEaTriX facility. The optical elements needed to generate (X-ray source), filter, polarize and expand the beam (parabolic mirror, collimators, symmetric crystals, asymmetric crystal) are all enclosed in the 5 m vacuum tube in the background and in the central tank ("short arm"). The 12 m vacuum tube (the "long arm") allows the ray to be focused on the detector. The short arm can be steered in the horizontal plane to fit the Bragg angle on the asymmetric crystal, while the long arm can be tilted vertically to fit the reflection angle of the facility under test.

Finally, all the system needs to be evacuated to avoid X-ray absorption in air. The total range of X-rays from source to detector at the end of the 12 m long tube is 17 m. Fortunately, the reduced dimensions of the facility require only a moderate vacuum level: a previous simulation[9] showed that even a 0.1 mbar residual pressure would suffice to preserve 75% of the beam intensity at 1.5 keV and more than 98% at 4.5 keV. In this design, four dry pumps can be used to reach a vacuum level of 10^{-2} mbar and independently evacuate four sections of the facility: of these, only the XOU vacuum tank will undergo a continuous venting/evacuation at the operation time, with a considerable time saving when the XOU under test is to be changed. All the system will be mounted in a ground-based laboratory at 20 °C temperature, stable within 1 °C. A clean tent (ISO4 class or better) mounted above the sample holder housing will allow us mounting/removing the XOU under test without dust contaminations.

3. ADVANCEMENT STATUS

3.1. The collimating mirror

As detailed in Sect. 2, the divergent X-ray beam is made parallel and expanded in the vertical direction by grazing reflection on a parabolic mirror. The figuring accuracy of the mirror is essential to guarantee high efficiency in the subsequent spectral filtering by the symmetric crystals. For this reason, the mirror needs to be highly polished and figured aiming at a maximum tolerable HEW of 3 arcsec, with excellent thermal stability and mechanically stable during the alignment. The material selected is fused quartz HOQ 310, a material easy to polish and figure to an excellent level, characterized by an extremely low level of impurities and inclusions, and very low coefficient of thermal expansion (0.5×10^{-6} K^{-1}).

The first step to be taken in the paraboloidal mirror development has been the determination of manufacturing tolerances: doing this, we are primarily interested in the longitudinal profile errors, because in grazing incidence the roundness errors have a lesser weight in the PSF broadening by two orders of magnitude. We have therefore created a number of simulated profile errors superimposing elementary harmonic components with spatial frequencies k/L, where L = 436 mm and k = 1, 2,… down to a spatial wavelength of 2 mm. The harmonic amplitudes are in proportion to the spatial periods, varying the relative phase of the components at random several times. The resulting profiles have been superimposed to rough profiles constructed from a PSD (power spectral density) in the shape of a power-law $P(f) = K_n/f^n$ in the bandwidth 1 mm – 10 μm with variable n and K_n parameters that have been varied – together with the amplitude/period ratio of the figure error components - until a slope value in agreement with the HEW < 3 arcsec requirement at E < 4.5 keV was found. Doing this, the PSF was computed from the modeled profiles using the WISE code[14] to self-consistently compute the PSF from figure error and roughness. The results are shown in Fig. 7; the tolerable values for the amplitude/period ratio of figure errors harmonic components is 1 μrad and roughness PSD below the power law-model with n = 1.05 and K_n = 18 $nm^3 \mu m^{-1.05}$, which mean a final surface quality σ_m < 3 μrad slope rms at spatial wavelengths larger than 2 mm, and a roughness rms σ < 2 Å at spatial periods smaller than 1 mm. One of the infinitely possible profile errors within the tolerances is shown in Fig. 8.

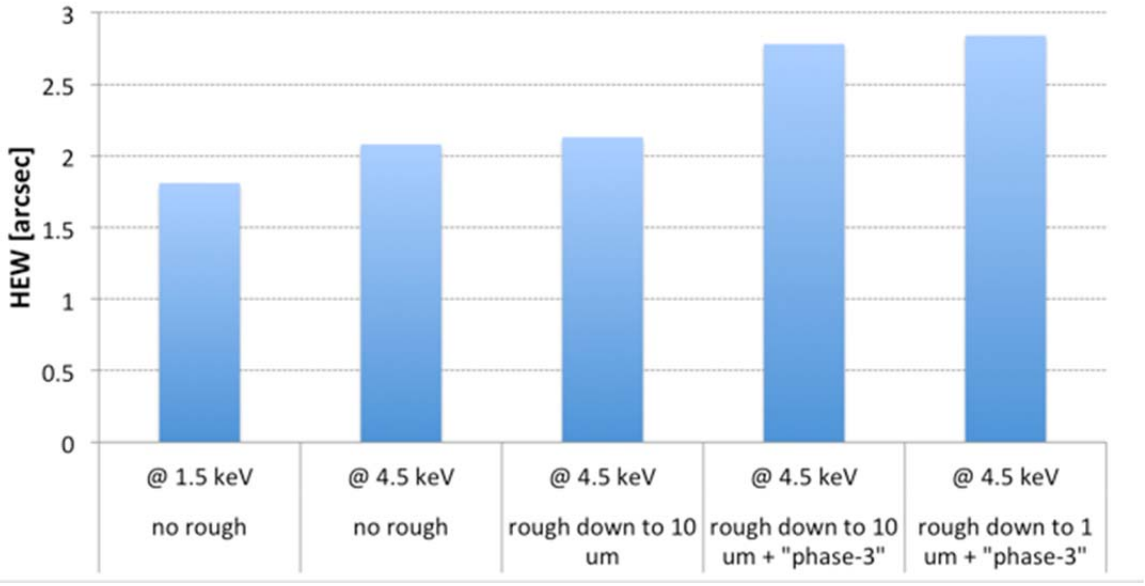

Fig. 7: mirror HEW expected from a proper combination of sinusoidal errors with spatial periods L (in mm) from mirror length down to 2 mm and amplitude linearly scaling as $L/4$ in nm, with and without the tolerable roughness PSD (assumed to be a power-law spectrum $P(f) = K_n/f^n$ with n = 1.05 and K_n = 18 $nm^3 \mu m^{-1.05}$). The component amplitudes have been selected with a maximum slope of 1 μrad, and the resulting HEW is always within the 3 arcsec tolerance.

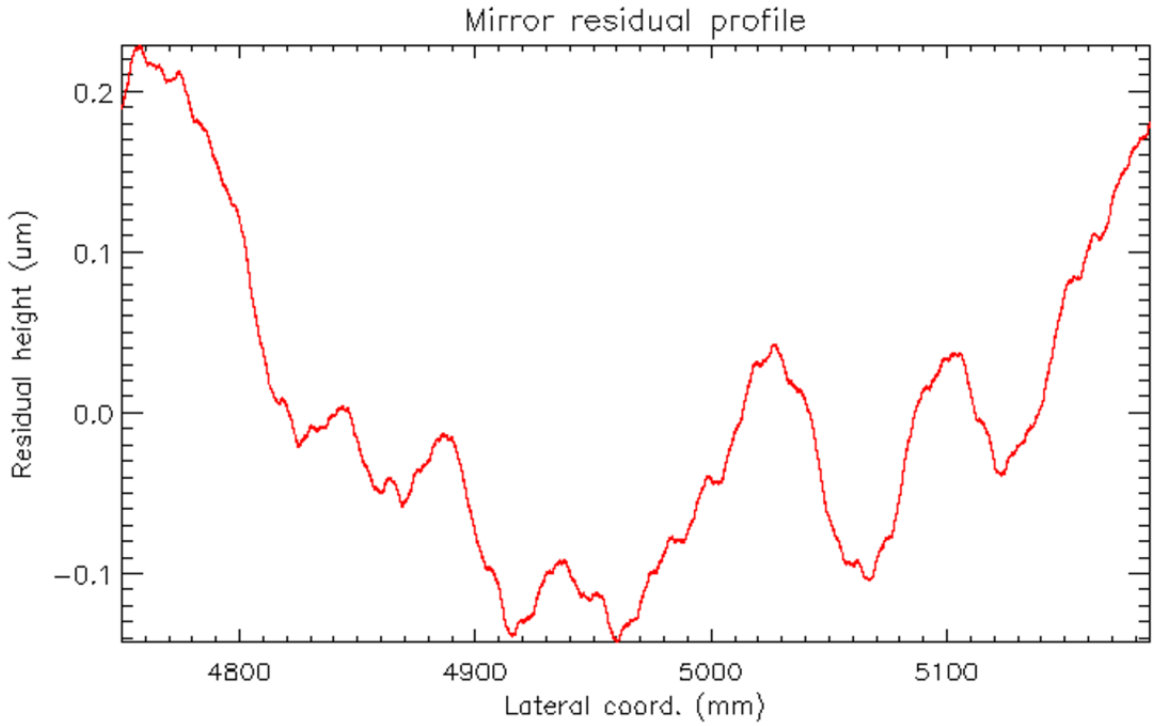

Fig. 8: one of the infinitely possible profile errors, obtained with 16 harmonics with constant slope errors of 1 μrad. This profiles gives us an idea of the tolerable figure error on the longitudinal profile of the mirror.

The paraboloidal mirror (Fig. 9) was purchased from Carl Zeiss SMT GmbH (Oberkochen, Germany), in a preliminary grinding (rms < 5 μm) and polishing (rms < 0.5 μm) status. The mirror has recently arrived to our labs, and a preliminary metrological analysis (Fig. 10, using an optical distance sensor mounted on our long trace profilometer stage) showed us that the mirror is within the preliminary grinding and lapping specifications. The finally required polishing level will be reached using the ZEEKO lapping machine installed at INAF/OAB, while the final shape accuracy can be obtained by Ion Beam Figuring using the dedicated facility at OAB[15]. Also a spare grinded mirror - without lapping – was procured from Zeiss to be polished and figured if needed. Initial tests with HOQ 310 samples are in progress at the ZEEKO facility at INAF/OAB and the first polishing cycle is expected to be started soon.

Fig. 9: one of the two paraboloidal mirrors procured from Carl Zeiss SMT GmbH, after the preliminary grinding. The mirror was subsequently lapped to remove the periodic pattern left by grinding.

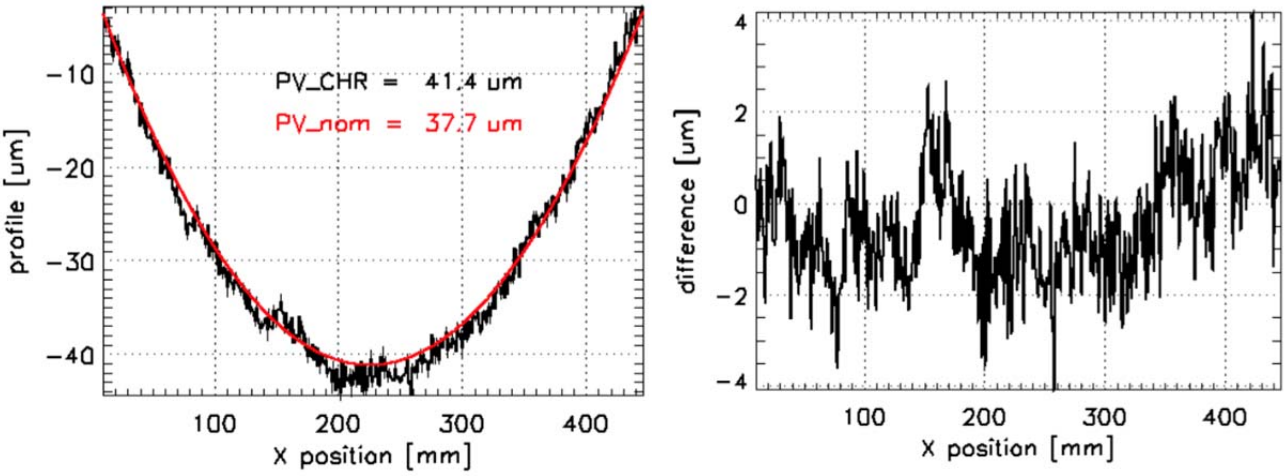

Fig. 10: preliminary metrology using the Crocodile sensor mounted on LTP at OAB, on the grinded and lapped mirror as procured from Zeiss. (left) measurement compared to the nominal profile. (right) the measured profile error. The high-frequency pattern will be removed by the polishing with the ZEEKO machine, while the low-frequency part is expected to be corrected by the IBF facility, both operated at OAB.

3.2. The asymmetric cut crystal

The asymmetric cut crystal for the 4.51 keV setup is also being fabricated. A 20 cm diameter, 5 cm high cylinder in monocrystalline silicon (Fig. 11) has been procured from MEMC. The silicon is extremely pure and the terminal faces of the cylinder correspond to the (100) plane orientation, therefore the (220) planes in the silicon cubic cell are oriented at 45 deg with respect to the terminal surfaces. The beam expander surface needs to form a 44.7 deg angle with the (220) planes, therefore the cut plane is just 0.3 deg off the cylinder terminal surface. A precise cut is required to ensure the correct expansion factor: the asymmetry angle has to be determined to a 0.1 deg uncertainty.

The crystal will be cut using the diamond saw facility operated at CNR-IMEM. The cutting procedure introduces a surface damage causing lattice damage at the crystal surface, which need to be removed by polishing. The polishing process allows the surface crystal to be smooth enough to be “visibly” shiny but not to an angstrom level of smoothness, as usually requested in grazing incidence optics (Sect. 3.1). Such a smoothness level, on the other hand, is not even required because the diffraction process does not occur at the surface but in the structure of the silicon crystal, that is largely unaffected by residual irregularities of the surface. The final performances of the asymmetric crystal will be directly tested in X-rays at CNR-IMEM.

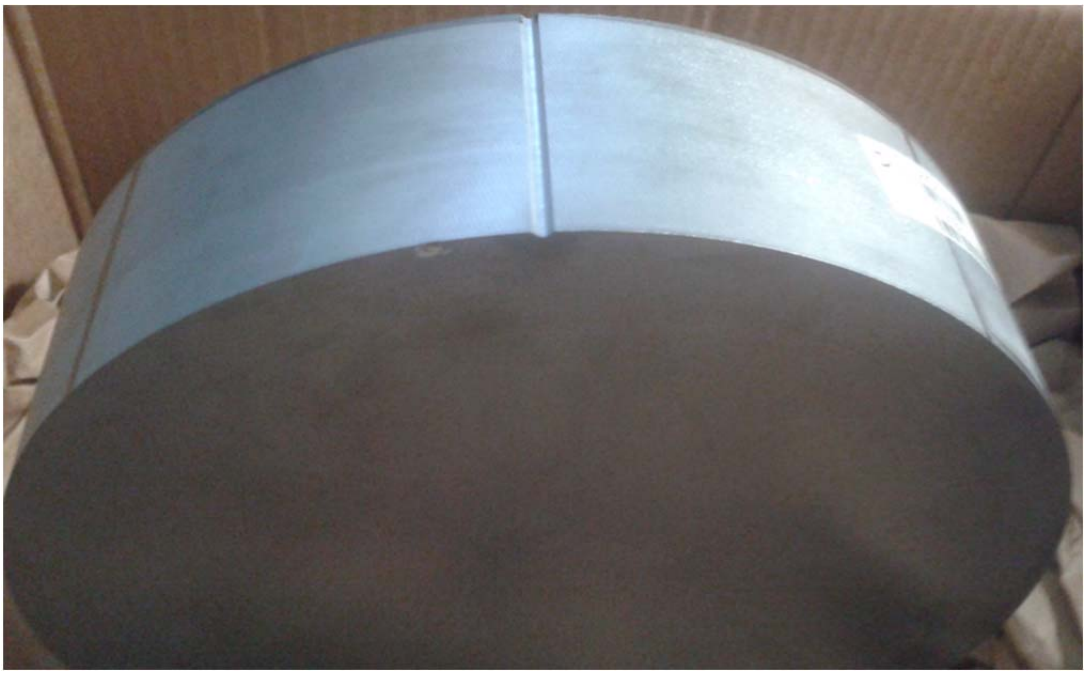

Fig. 11: the monocrystalline cylinder in silicon purchased from MEMC (20 cm diameter. 50 mm thick). The terminal surfaces are the planes (100). The lateral groove locates the (010) planes.

3.3. The laboratory

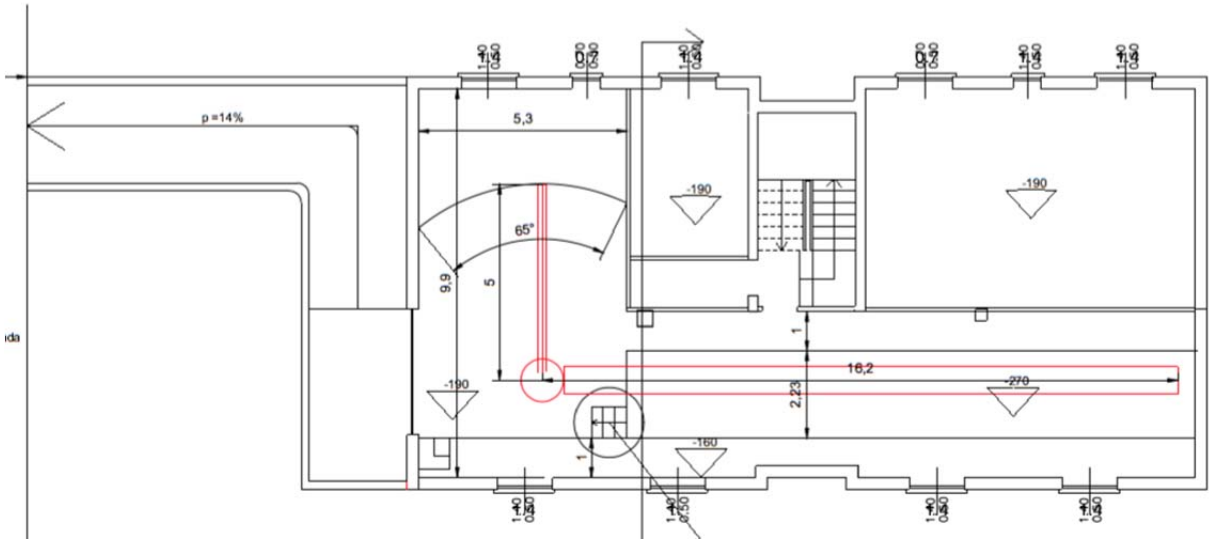

Fig. 12: design of the new laboratory, to be realized on the basement of an existing building. The BEaTriX facility planned location is drawn in red.

Even if BEaTriX will fits in a small laboratory, this is to be set up properly. The location has been determined as the basement of one of the buildings of INAF-OAB, Merate, formerly a house for the INAF-OAB personnel and currently being turned into laboratories. The underground floor is based on ground and the plans for the renovation and the change of utilization (Fig. 12) are currently complete. The short arm (Sect. 2.2) will be accommodated in one of the existing rooms and, by joining some other rooms, the length of the long arm will conveniently fit the residual space. An outer ramp will also be constructed to pass BEaTriX components (including vacuum tubes) directly from the outer space, once the laboratory is complete.

4. References

[1] Burwitz, V., Bavdaz, M., Pareschi, G., et al., "In focus measurements of IXO type optics using the new PANTER x-ray test facility extension," Proc. SPIE 8861, 88611J (2013)
[2] Miyazawa, T., Furuzawa, A., Kanou, Y., et al., "Current status of hard x-ray characterization of ASTRO-H HXT at SPring-8," Proc. SPIE 7732, 77323I (2010)
[3] Bavdaz, M., Wille, E., Shortt, B., et al., "The ATHENA optics development," Proc. SPIE 9905, 990525 (2016)
[4] Collon, M.J., Vacanti, G., Günther, R., et al., "Silicon pore optics for the ATHENA telescope," Proc. SPIE 9905, 990528 (2016)
[5] Spiga, D., Christensen, F., Bavdaz, M., et al., "Simulation and modeling of silicon pore optics for the ATHENA X-ray telescope," Proc. SPIE 9905, 99055O (2016)
[6] Vacanti, G., Ackermann, M., Vervest, M., et al., "X-ray pencil beam characterization of silicon pore optics," Proc. SPIE 8861, 88611K (2013)
[7] Menz, B., Brauninger, H., Burwitz, V., Hartner, G., Predehl, P., "Studying ATHENA optics with divergent and collimated x-ray beams," Proc. SPIE 9144, 91445J (2014)
[8] Spiga, D., Pareschi, G., Pelliciari, C., et al., "Functional tests of modular elements of segmented optics for x-ray telescopes via an expanded beam facility," Proc. SPIE 8443, 84435F (2012)
[9] Spiga, D., Pelliciari, C., Bonnini, E., et al., "An expanded x-ray beam facility (BEaTriX) to test the modular elements of the ATHENA optics," Proc. SPIE 9144, 91445I (2014)
[10] Pelliciari, C., Spiga, D., Bonnini, E., et al., "BEaTriX, expanded soft x-ray beam facility for test of focusing optics, an update," Proc. SPIE 9603, 96031P (2015)
[11] Cotroneo, V., Spiga, D., Bruni, R., et al., "New developments in light material overcoating for soft x-ray reflectivity enhancement," Proc. SPIE 7011, 701119 (2008)
[12] Fabiani, S., Costa, E., Del Monte, E., Muleri, F., et al., "The imaging properties of the Gas Pixel Detector as a focal plane polarimeter," Ap.J. Supplement Series 212, 25 (2014)
[13] Christensen, F., Hornstrup, A., Frederiksen, P., et al., "Expanded beam x-ray optics calibration facility at the Daresbury Synchrotron," Proc. SPIE 2011, 540 (1994)
[14] Raimondi, L., Spiga, D., "Mirrors for X-ray telescopes: Fresnel diffraction-based computation of point spread functions from metrology," A&A 573, A22 (2015)
[15] Ghigo, M., Basso, S., Civitani, M., et al., "Ion beam figuring of large prototype mirror segments for the EELT," Proc. SPIE 9151, 91510Q (2014)